Equilibrium Spin Configuration and Resonance Behavior of $RbMnF_3$

PETER H. COLE
Department of Electrical Engineering and Center for Materials Science and Engineering, Massachusetts Institute of Technology, Cambridge, Massachusetts*

AND

WILLIAM J. INCE
Lincoln Laboratory, Massachusetts Institute of Technology, Lexington, Massachusetts*

(Received 3 May 1966)

The equilibrium orientations of the magnetic sublattices of the cubic antiferromagnet $RbMnF_3$ have been studied. By assuming spatially uniform magnetization and restricting the applied steady magnetic field to lie in a {110} plane, the problem is considerably simplified. The analysis enables the equilibrium spin configurations for the important cases of the magnetizing field applied along any of the three principal crystal axes to be predicted. Each case has more than one solution. The theory predicts that abrupt spin flopping from one equilibrium state to another should occur under certain conditions. An antiferromagnetic-resonance theory is presented which is applicable over a wide range of field and embraces the low- and high-field resonance theories previously reported as restricted examples. Observations of the resonance spectrum at X-band frequencies for the applied field range 0 to 12 kOe are presented. The measurements provide excellent verification of the resonance theory and confirm the validity of the equilibrium analysis. The best fit between theory and experiment was obtained by assuming values of the anisotropy field significantly different from the previously published value. Abrupt spin flopping was not observed. The resonance data indicate that the magnetization can switch between equilibrium directions gradually over a range of field and at much lower field strengths than the theoretical flopping field.

I. INTRODUCTION

THE antiferromagnetic properties of the perovskite $RbMnF_3$ were first reported by Teaney *et al.*[1] In this material the Mn^{2+} ions are distributed on a cubic lattice, the lattice constant being 4.24 Å. Below the Néel temperature of 82.6°K the spins form a two-sublattice antiparallel configuration. The antisotropy appears to be wholly cubic, the [111] directions being equivalent easy directions.

Apart from the insight it provides into the magnetic structure of the material, a detailed knowledge of the equilibrium direction of the sublattice magnetizations is necessary for many experiments. For example, in the measurement of magnetoelastic constants[2] it is necessary to confine the magnetization to lie along a particular direction with respect to the applied mechanical strain. Another example is the measurement of the spin-wave linewidth[3] by the method of parallel pumping,[4] which requires that the magnetization and the rf pumping field be parallel.

As a consequence of the four-fold degeneracy of the anisotropy energy surface in $RbMnF_3$, there is no unique direction for the sublattice magnetizations in the absence of an applied steady field, in which case the spins may be distributed along the four [111] axes. For weak applied fields, the equilibrium direction of the sublattices is also multivalued. However, for fields in excess of about 8 kOe, the spins are almost orthogonal to the field. They are free to rotate in the plane perpendicular to the applied field $\mathbf{H}_0$ and assume the direction of the anisotropy minimum within that plane. Hence, for the high-field case, the equilibrium direction of the magnetization is well defined. Teaney *et al.*[1] and Freiser *et al.*[5,6] have made use of the high-field modes to investigate the antiferromagnetic-resonance (AFMR) spectrum. The advantage of this configuration is that it is readily amenable to analysis. Their theory predicts two resonance modes, one of which is independent of the magnitude of H_0.[6] The latter is excited by applying the rf field parallel to $\mathbf{H}_0$ while the field-dependent mode is excited by a field perpendicular to $\mathbf{H}_0$. By comparing the predicted resonances with the experimental values, measured as a function of the applied field direction with respect to the crystal axes, the anisotropy and exchange fields were found to be 4.47 and 8.9×10^5 Oe, respectively, at 4.2°K.

The low-field region has been investigated by Ince.[3,7] He attempted to predict the equilibrium direction of the sublattice magnetization under the influence of an applied steady field for a restricted but useful range of field directions. By assuming $\mathbf{H}_0$ and the sublattice magnetizations $\mathbf{M}_1$ and $\mathbf{M}_2$ to lie in the (110) plane, a simple transcendental equation was obtained, the solution of which gave the equilibrium direction. A resonance analysis was performed which made use of the predictions of the simple model to calculate the normal mode frequencies. Although agreement was obtained at low fields between theory and the limited experimental

* Operated with support from the U. S. Advanced Research Projects Agency.

[1] D. T. Teaney *et al.*, Phys. Rev. Letters **9**, 212 (1962).
[2] D. E. Eastman, J. Appl. Phys. **37**, 996 (1966).
[3] W. J. Ince, S. M. thesis, MIT, 1965 (unpublished).
[4] F. R. Morgenthaler, J. Appl. Phys. **36**, 3102 (1965).
[5] M. J. Freiser *et al.*, *Proceedings of the International Conference on Magnetism, Nottingham, 1964* (Institute of Physics and the Physical Society, London, 1965), p. 432.
[6] M. J. Freiser *et al.*, Phys. Rev. Letters **10**, 293 (1963).
[7] W. J. Ince, J. Appl. Phys. **37**, 1132 (1966).

data for two of the principal crystal axes, it could not account for the observed low-field resonances with the applied field parallel to the [110] axis. Moreover, the theory completely failed to predict the high field modes previously reported.[5,6] The purpose of this paper is to present an improved analysis of the equilibrium problem which accounts for the discrepancies of the earlier work. The resonance theory has been refined in detail by including significant terms in the equations of motion omitted previously, and successfully predicts all of the low field resonance modes in addition to the flopped modes. The experimental measurements have been greatly extended, and permit a detailed comparison with the theory to be made.

II. EQUILIBRIUM ORIENTATION OF THE MAGNETIC SUBLATTICES

If a single crystal of $RbMnF_3$ is cooled below its Néel temperature in the absence of a magnetic field, some distribution of the magnetization along the four easy axes can be anticipated.[8] The detailed manner in which the magnetization distributes itself is determined by the impurities, dislocations, and inhomogeneities which, as Keffer and Kittel[9] have pointed out, play an important role in determining the spin configuration in antiferromagnets. Néel[8] has predicted the occurrence of domains in cubic antiferromagnets, but has pointed out that they are likely to be ill-defined because energy terms favoring their formation are small. Despite these complications we shall proceed on the assumption of uniform magnetization. This simplification seems reasonable in view of the extent of agreement obtained between the theory which is based on this assumption and the experimental results.

The case of the steady field applied along one of the three principal crystal axes will now be considered. The principal axes for the cubic geometry are illustrated in Fig. 1, together with the relevant angles between them. Suppose $\mathbf{H}_0$ to be along the [001] axis. At zero field the magnetization can lie along any of the four [111] axes at an angle α with respect to $\mathbf{H}_0$, as shown in Fig. 2(a). As the magnitude of $\mathbf{H}_0$ is increased, the magnetization

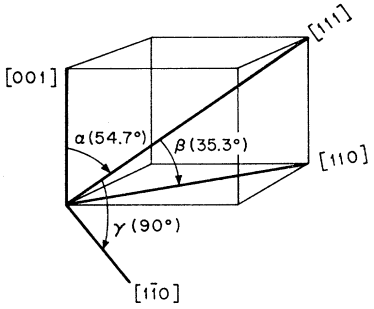

FIG. 1. Notation for the cubic geometry.

[8] L. Néel, *Proceedings of the International Conference on Theoretical Physics 1953* (Tokyo, Japan, 1954), p. 701.
[9] F. Keffer and C. Kittel, Phys. Rev. **85**, 2 (1952).

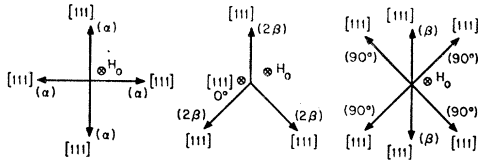

(a) H_0 PARALLEL TO[001]AXIS (b) H_0 PARALLEL TO[111]AXIS (c) H_0 PARALLEL TO[110]AXIS

FIG. 2(a). Low-field equilibrium orientations of $\mathbf{M}$ with $\mathbf{H}_0$ along [001]. (b) Low-field equilibrium orientations of $\mathbf{M}$ with $\mathbf{H}_0$ along [111]. (c) Low-field equilibrium orientations of $\mathbf{M}$ with $\mathbf{H}_0$ along [110].

rotates away from the field. Eventually, for very large fields the magnetization must be along any of the four [110] axes perpendicular to the [001] axis. In addition the magnetization is canted slightly towards $\mathbf{H}_0$ by a small tilt angle equal to $H_0/2H_{ex}$ rad which is ignored for the moment.

Now suppose a small field $\mathbf{H}_0$ is applied along a [111] axis. The configuration possesses a threefold symmetry as in Fig. 2(b). The magnetization along any of the three axes, at an angle 2β with the field direction, rotates away from $\mathbf{H}_0$ with increasing field strength. At high fields the angle 2β is replaced by 90° in Fig. (2b). A second possibility exists for this case, namely that the magnetization could initially be parallel to $\mathbf{H}_0$. It will be shown that at high fields this position is unstable and the approximately perpendicular orientations have a lower energy state.

In Fig. 2(c) the field is applied along the [110] axis, which has twofold symmetry. Two [111] directions make an angle β with respect to the field. With increasing field strength, the magnetization along these axes will rotate initially towards the [001] axis. There are also two [111] axes perpendicular to the field as illustrated in the diagram, and the magnetization along either of these directions remains perpendicular to the field over the entire range of $\mathbf{H}_0$.

From the foregoing discussion it appears that when $\mathbf{H}_0$ is applied along a principal crystal axis, the equilibrium orientation of the sublattices must lie in a (110) plane. Further, except when $\mathbf{H}_0$ is in a [110] direction, for which there are two perpendicular [111] axes, $\mathbf{H}_0$, $\mathbf{M}_1$, and $\mathbf{M}_2$ must lie in the same (110) plane. Hence the analysis will proceed on the assumption of a simple (110) plane model.

Analysis of the (110)-Plane Model

The model is illustrated in Fig. 3. The equilibrium direction makes an angle θ with respect to the [001] axis. The sublattice magnetizations $\mathbf{M}_1$ and $\mathbf{M}_2$ are each tilted out of the equilibrium direction by an angle t towards the direction of $\mathbf{H}_0$ which makes an angle ψ with the [001] axis. The equilibrium direction is defined by the vector $\mathbf{M}$, where $\mathbf{M}=(\mathbf{M}_1-\mathbf{M}_2)/2$.

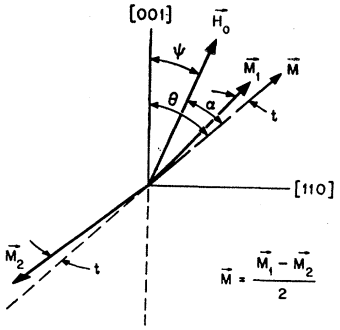

FIG. 3. Coordinate system for analysis of equilibrium orientations.

The anisotropy energy is given by

$$\mathcal{H}_{\text{anis}} = -\tfrac{1}{4}K\{\sin^4(\theta-t)+\sin^2 2(\theta-t) + \sin^4(\theta+t)+\sin^2 2(\theta+t)\},$$

where the anitotropy constant K is positive.

The exchange energy is

$$\mathcal{H}_{\text{ex}} = -\mu_0 w_{12}\mathbf{M}_1\cdot\mathbf{M}_2 = \mu_0 w_{12} M^2\cos 2t,$$

where $M_1 = M_2 = M$ and $|w_{12}|M = \mathbf{H}_{\text{ex}}$.

The Zeeman energy

$$\mathcal{H}_Z = -\mu_0(\mathbf{M}_1+\mathbf{M}_2)\cdot\mathbf{H}_0 = -\mu_0 M H_0\{\cos(\theta-\psi-t)-\cos(\theta-\psi+t)\} = -2\mu_0 M H_0 \sin(\theta-\psi)\sin t.$$

The total free energy, which is the sum of the anisotropy, exchange, and Zeeman terms, is minimized with respect to the tile angle t. On performing the differentiation and using the small angle approximations for $\sin t$ and $\cos t$, we find that

$$t = \frac{H_0\sin(\theta-\psi)}{2\{H_{\text{ex}}+(3H_a/16)(2\cos 2\theta+\cos 4\theta)\}},$$

where H_a is the effective anisotropy field along the [111] axis. The term in H_a can be dropped, since $H_a/H_{\text{ex}} \approx 10^{-5}$ here. Hence,

$$t = (H_0\sin(\theta-\psi)/2H_{\text{ex}}). \quad (1)$$

It is seen that because of the relative magnitudes of H_a and H_{ex}, the tilt angle is almost independent of the anisotropy.

After substitution of the above expression for t in the free energy terms, the total free energy is minimized with respect to θ. The resulting transcendental equation is

$$(-4H_0^2/3H_{\text{ex}}H_a)\sin 2(\theta-\psi) = \sin 2\theta(1+3\cos 2\theta) \quad (2)$$

and the total free energy at equilibrium is given by

$$\mathcal{H}_{\text{equil.}} = -\mu_0 M\{H_{\text{ex}}+(H_0^2/2H_{\text{ex}})\sin^2(\theta-\psi) + \tfrac{3}{8}H_a(\sin^4\theta+\sin^2 2\theta)\}. \quad (3)$$

Solutions to Eq. (2) have been plotted in Fig. 4 for $\mathbf{H}_0$ applied along the three principal axes and also for some intermediate directions.

Case 1. H_0 Parallel to a [111] Axis ($\psi = 54.7°$)

If the magnetization is initially along the same [111] axis as $\mathbf{H}_0$, it will remain along that direction as the field strength is increased until the field reaches the value $(2H_{\text{ex}}H_a)^{1/2}$. The equilibrium direction then abruptly switches or flops to the adjacent quadrant of the (110) plane. Further increase in H_0 causes further rotation of the equilibrium direction until for very large field strengths $\mathbf{M}$ and $\mathbf{H}_0$ are almost orthogonal. Reduction of H_0 below the value $(2H_{\text{ex}}H_a)^{1/2}$ does not cause $\mathbf{M}$ to flop back again and at zero field $\mathbf{M}$ is located along the [111] axis in the adjacent quadrant of the (110) plane.

Case 2. H_0 Parallel to [001] Axis ($\psi = 0°$)

The magnetization rotates away from the [111] direction with increasing H_0 until at a value of $(1.5H_{\text{ex}}H_a)^{1/2}$ the sublattices are almost perpendicular to the field, but canted towards the [001] axis by a tilt angle equal to $H_0/2H_{\text{ex}}$ rad. On reducing the field the magnetization rotates smoothly back to the [111] axis. Flopping is not predicted.

Case 3. H_0 Parallel to [110] Axis ($\psi = 90°$)

We consider rotation of $\mathbf{M}$ within the (110) plane containing $\mathbf{H}_0$, and out of this plane. Symmetry considerations demand that with respect to rotation of $\mathbf{M}$ out of this plane, the in-plane position has at least a stationary value of energy, but is possibly unstable. As the field is increased, the equilibrium position rotates in the plane away from the [111] direction, the in-plane position initially remaining stable. The theory predicts that for field strengths greater than $(3H_{\text{ex}}H_a)^{1/2}$ the equilibrium direction will be parallel to the [001] axis. However, this is a hard direction and is therefore an unstable equilibrium. At some direction between [111]

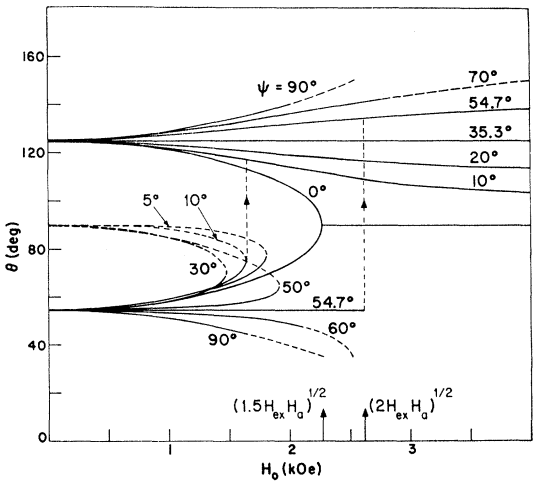

FIG. 4. Computed position of $\mathbf{M}$ as a function of magnitude and direction of $\mathbf{H}_0$ in the (110) plane.

and [001] the in-plane position becomes unstable, and the magnetization moves to the [111] direction orthogonal to the steady field. This location is an absolute energy minimum for all values of H_0.

Since to a very good approximation, the total free energy may be expressed as the sum of noninteracting Zeeman, exchange and anisotropy contributions the value of θ at which the in-plane equilibrium direction becomes unstable is readily found by considering the change in anisotropy energy as $\mathbf{M}$ is rotated out of the plane, with the angle between $\mathbf{M}$ and $\mathbf{H}_0$ held constant. In this manner the critical value of θ was calculated to be 140.5° (or 39.5°).

Case 4. H_0 Along an Arbitrary Direction

Figure 4 shows the predicted equilibrium orientations for directions of $\mathbf{H}_0$ other than the three principal directions. For values of ψ between 0° and 54.7° the curves are multivalued as a function of H_0. The dashed portions represent unstable regions. The point where a curve reaches its maximum value in field corresponds to the field at which the magnetization flops to the adjacent quadrant of the (110) plane. Note that the field required for flopping varies rapidly as a function of angle, and that upon removal of the field the magnetization does not necessarily return to its original position. If spin flopping does in fact occur (although this effect has not yet been observed in $RbMnF_3$), its observation requires careful prepositioning of $\mathbf{M}$ and an accurately aligned uniform applied field.

III. RESONANCE ANALYSIS

A. Equation of Motion

The assumptions of cubic anisotropy, an isotropic exchange interaction and the gyromagnetic equation, lead to the linearized equations of motion for the sublattices.[3] They can be expressed in the following form:

$$j\omega\begin{bmatrix}\boldsymbol{\alpha}_1\\ \boldsymbol{\alpha}_2\end{bmatrix}=\begin{bmatrix}\mathbf{A}_{11}{}^c+\mathbf{B}_{11}{}^c & \mathbf{C}_{12}{}^c\\ \mathbf{C}_{21}{}^c & \mathbf{A}_{22}{}^c+\mathbf{B}_{22}{}^c\end{bmatrix}\begin{bmatrix}\boldsymbol{\alpha}_1\\ \boldsymbol{\alpha}_2\end{bmatrix}. \quad (4)$$

Vectors $\boldsymbol{\alpha}_1$ and $\boldsymbol{\alpha}_2$ are the rf magnetizations of sublattices 1 and 2 in the cubic crystal axis coordinate system (ξ,η,ζ), with axes along [100], [010], [001] directions, respectively. Elements of the arrays $\mathbf{A}_{11}{}^c$, $\mathbf{B}_{11}{}^c$, etc., the first of which describes anisotropy effects, are

$$\mathbf{A}_{11}{}^c=\frac{2K\gamma}{M^4}\begin{pmatrix}0 & 3M_{1\xi}M_{1\eta}{}^2-M_{1\zeta}{}^3 & -3M_{1\eta}M_{1\zeta}{}^2+M_{1\eta}{}^3\\ -3M_{1\zeta}M_{1\xi}{}^2+M_{1\zeta}{}^3 & 0 & 3M_{1\xi}M_{1\zeta}{}^2-M_{1\xi}{}^3\\ 3M_{1\eta}M_{1\xi}{}^2-M_{1\eta}{}^3 & -3M_{1\xi}M_{1\eta}{}^2+M_{1\xi}{}^3 & 0\end{pmatrix}$$

$$\mathbf{B}_{11}{}^c=\gamma\mu_0\begin{pmatrix}0 & H_{1\zeta}+w_{12}M_{2\zeta} & -H_{1\eta}-w_{12}M_{2\eta}\\ -H_{1\zeta}-w_{12}M_{2\zeta} & 0 & H_{1\xi}+w_{12}M_{2\xi}\\ H_{1\eta}+w_{12}M_{2\eta} & -H_{1\xi}-w_{12}M_{2\xi} & 0\end{pmatrix}$$

$$\mathbf{C}_{12}{}^c=\gamma\mu_0\begin{pmatrix}0 & -w_{12}M_{1\zeta} & w_{12}M_{1\eta}\\ w_{12}M_{1\zeta} & 0 & -w_{12}M_{1\xi}\\ -w_{12}M_{1\eta} & w_{12}M_{1\xi} & 0\end{pmatrix}.$$

In the above, $\mathbf{H}_1$ contains the applied field $\mathbf{H}_0$ and the effective nuclear field[1] $\mathbf{H}_{1n}$ which is directed along $\mathbf{M}_1$.

B. Transformation of Equations of Motion

Three new coordinate systems defined in Fig. 5 assist in simplifying the equations of motion. For each system the z and x axes are in the (110) plane, the z, z^1, and z^2 axes coinciding with the $\mathbf{M}$, $\mathbf{M}_1$, and $\mathbf{M}_2$ directions, respectively.

The transformation from (ξ,η,ζ) to (x,y,z) is $\mathbf{x}=\mathbf{T}\cdot\boldsymbol{\xi}$, where

$$T=\begin{bmatrix}(\cos\theta)/\sqrt{2} & (\cos\theta)/\sqrt{2} & -\sin\theta\\ -1/\sqrt{2} & 1/\sqrt{2} & 0\\ (\sin\theta)/\sqrt{2} & (\sin\theta)/\sqrt{2} & \cos\theta\end{bmatrix}.$$

The transformation from (x,y,z) to (x^1,y^1,z^1) and (x^2,y^2,z^2) are the rotations $\mathbf{R}(-t)$, $\mathbf{R}(t)$ about the y axis by angles $-t$ and t, respectively.

The sublattice 1, 2 components of rf magnetization are transformed to the respective new coordinate systems by

$$\begin{bmatrix}\mathbf{a}_1\\ \mathbf{a}_2\end{bmatrix}=\begin{bmatrix}\mathbf{R}(-t)\cdot\mathbf{T} & 0\\ 0 & \mathbf{R}(t)\cdot\mathbf{T}\end{bmatrix}\begin{bmatrix}\boldsymbol{\alpha}_2\\ \boldsymbol{\alpha}_2\end{bmatrix}.$$

The resulting set of equations is

$$j\omega\begin{bmatrix}\mathbf{a}_1\\ \mathbf{a}_2\end{bmatrix}=\begin{bmatrix}\mathbf{A}_{11}{}^1+\mathbf{B}_{11}{}^1 & \mathbf{C}_{12}{}^1\cdot\mathbf{R}(2t)\\ \mathbf{C}_{21}{}^2\cdot\mathbf{R}(-2t) & \mathbf{A}_{22}{}^2+\mathbf{B}_{22}{}^2\end{bmatrix}\begin{bmatrix}\mathbf{a}_1\\ \mathbf{a}_2\end{bmatrix}. \quad (5)$$

The arrays, $\mathbf{A}_{11}{}^1$, $\mathbf{B}_{11}{}^1$, $\mathbf{C}_{12}{}^1$, etc., are the result of transforming $\mathbf{A}_{11}{}^c$, etc. from the crystal axis system to the (x^1,y^1,z^1) system by unitary transformations of the

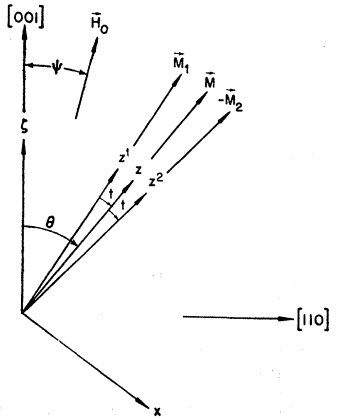

FIG. 5. Coordinate systems for the analysis of resonant frequencies.

type $\mathbf{B}_{11}{}^{1}=\mathbf{R}(-t)\cdot\mathbf{T}\cdot\mathbf{B}_{11}{}^{c}\cdot\mathbf{T}^{-1}\cdot\mathbf{R}^{-1}(-t)$. For all arrays except the $\mathbf{A}_{11}{}^{c}$ and $\mathbf{A}_{22}{}^{c}$ the transformed ones can be written down at sight.

The set of Eqs. (5) are reduced to a set of four by omitting the $a_{1z}{}^{1}$ and $a_{2z}{}^{2}$ components, which vanish in a first-order analysis. The remaining equations are

$$j\omega\begin{bmatrix}\mathbf{a}_1\\ \mathbf{a}_2\end{bmatrix}=\begin{bmatrix}\mathbf{A}+\mathbf{D}+\mathbf{E} & \mathbf{C}\\ -\mathbf{C} & -\mathbf{A}-\mathbf{D}+\mathbf{E}\end{bmatrix}\begin{bmatrix}\mathbf{a}_1\\ \mathbf{a}_2\end{bmatrix}. \quad (6)$$

The new arrays have the components

$$\mathbf{C}=H_{ex}\begin{bmatrix}0 & 1\\ -\cos 2t & 0\end{bmatrix}\gamma\mu_0,$$

$$\mathbf{D}=\gamma\mu_0(H_{ex}+H_n)\mathbf{J},$$

where

$$\mathbf{J}=\begin{bmatrix}0 & 1\\ -1 & 0\end{bmatrix} \quad \text{and} \quad H_n=H_{1n}=H_{2n},$$

and

$$\mathbf{E}=\gamma\mu_0 H_0\cos(\theta-\psi)\mathbf{J}.$$

The anisotropy array $\mathbf{A}^{c}$ when transformed to the (x,y,z) system becomes

$$\mathbf{A}=\begin{bmatrix}0 & a_{12}\\ a_{21} & 0\end{bmatrix},$$

where

$$a_{12}=-\tfrac{3}{2}\gamma\mu_0 H_a(1-\tfrac{7}{2}\sin^2\theta+\tfrac{3}{2}\sin^4\theta),$$

and

$$a_{21}=\tfrac{3}{2}\gamma\mu_0 H_a(1-(13/2)\sin^2\theta+6\sin^4\theta). \quad (7)$$

Since the anisotropy terms are much less in magnitude than the others in Eq. (5) and the tilt angle t is very small, these expressions are a sufficient approximation to the components of the anisotropy tensor in the (x^1,y^1,z^1) and (x^2,y^2,z^2) systems.

C. Normal-Mode Frequencies

The resonant frequencies of the modes are given by the determinantal equation

$$\begin{vmatrix}\mathbf{A}+\mathbf{D}+\mathbf{E}-j\omega\mathbf{I} & \mathbf{C}\\ -\mathbf{C} & -\mathbf{A}-\mathbf{D}+\mathbf{E}-j\omega\mathbf{I}\end{vmatrix}=0.$$

Since $|\mathbf{C}|\neq 0$, the equation can be put in the alternative form

$$\begin{vmatrix}\mathbf{I} & \mathbf{C}^{-1}(\mathbf{A}+\mathbf{D}+\mathbf{E}-j\omega\mathbf{I})\\ \mathbf{C}^{-1}(\mathbf{A}+\mathbf{D}-\mathbf{E}+j\omega\mathbf{I}) & \mathbf{I}\end{vmatrix}=0$$

which can be reduced to an equation involving a 2×2 determinant:

$$|\mathbf{I}-\mathbf{C}^{-1}(\mathbf{A}+\mathbf{D}+\mathbf{E}-j\omega\mathbf{I})\mathbf{C}^{-1}(\mathbf{A}+\mathbf{D}-\mathbf{E}+j\omega\mathbf{I})|=0.$$

Expansion of these matrix products is facilitated by writing

$$\mathbf{C}^{-1}=(+1/\omega_{ex})(\mathbf{J}+\mathbf{P})$$

where

$$\mathbf{P}=\begin{bmatrix}0 & \dfrac{2\sin^2 t}{\cos 2t}\\ 0 & 0\end{bmatrix}.$$

$\mathbf{P}$ is so small that only its product with $\mathbf{D}$ produces terms sufficiently large to be retained. When the product is formed, we obtain

$$\left|\omega_{ex}{}^{2}\mathbf{I}-\begin{bmatrix}+\omega_{ex}\mathbf{I} & +\omega_{ex}\mathbf{I}\\ +\omega_0\cos\varphi\mathbf{I}-j\omega\mathbf{J} & -\omega_0\cos\varphi\mathbf{I}+j\omega\mathbf{J}\\ -\omega_{ex}\mathbf{P}\cdot\mathbf{J}+\mathbf{J}\cdot\mathbf{A}+\omega_n\mathbf{I} & -\omega_{ex}\mathbf{P}\cdot\mathbf{J}+\mathbf{J}\cdot\mathbf{A}+\omega_n\mathbf{I}\end{bmatrix}\right|=0,$$

where $\varphi=(\theta-\psi)$, $\omega_{ex}=-\gamma\mu_0 H_{ex}$, $\omega_0=-\gamma\mu_0 H_0$, and $\omega_n=-\gamma\mu_0 H_n$.

In the remaining matrix multiplication all terms of the magnitude of ω^2, $\omega_{ex}\omega_a$, $\omega_0{}^2$, but no smaller, are retained. The result, on expanding the determinant, is the biquadratic equation

$$(\omega^2-\omega_+{}^2)(\omega^2-\omega_-{}^2)-4\omega^2\omega_0{}^2\cos^2\varphi=0 \quad (8)$$

where

$$\omega_+{}^2=2\omega_{ex}(\omega_n+a_{21})+\omega_0{}^2(2\sin^2\varphi-1),$$

and

$$\omega_-{}^2=2\omega_{ex}(\omega_n-a_{12})+\omega_0{}^2(\sin^2\varphi-1).$$

When the magnetization equilibrium direction is orthogonal to the applied field, the equation gives the field-tuned mode and the field-independent mode as found by Freiser, *et al.*[5] By retaining higher order terms in t than were used in a previous derivation of this spectrum,[3,7] a somewhat different result has been obtained.

D. Resonances with H_0 Along Principal Directions

Normal mode frequencies as functions of applied steady field were obtained by using a computer to solve first for the equilibrium orientations, as given by Eq.

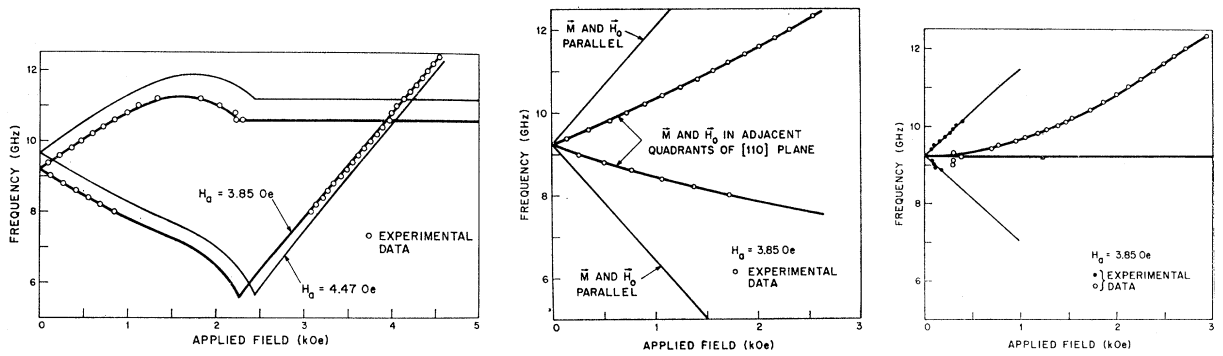

FIG. 6. (a) Theoretical mode spectra and experimental results for the Sperry sample with $\mathbf{H}_0$ along [001]. The solid lines represent the theoretical modes predicted by the single domain model. Best fit to the experimental data is obtained by assuming $H_{ex}=8.9\times10^5$ Oe and $H_a=3.85$ Oe. (b) Theoretical mode spectra and experimental results for the Sperry sample with $\mathbf{H}_0$ along [111]. $H_{ex}=8.9\times10^5$ Oe, $H_a=3.85$ Oe. (c) Theoretical mode spectra and experimental results for the Sperry sample with $\mathbf{H}_0$ along [110]. $H_{ex}=8.9\times10^5$ Oe, $H_a=3.85$ Oe.

(2), and then for the resonant frequencies, as given by Eq. (8). Mode spectra for $\mathbf{H}_0$ applied along the [100], [110], and [111] directions are shown as the solid lines in Figs. 6a to 6c. The values of anisotropy and exchange fields used in the computation are 3.85 and 8.9×10^5 Oe, respectively. For each equilibrium orientation of $\mathbf{M}$, two resonant frequencies occur. For a single domain theory, with sufficiently low values of $\mathbf{H}_0$ in the [111] direction, two stable positions of $\mathbf{M}$ are possible and the mode spectrum has four branches. At high fields there is only one stable equilibrium position and therefore only a two branched spectrum, with slopes tending to zero and $\gamma/2\pi$, respectively, as H_0 becomes large.

When $\mathbf{H}_0$ is in the [110] direction, the equilibrium direction of $\mathbf{M}$ is along a [111] axis orthogonal to $\mathbf{H}_0$ but not in the same (110) plane; the appropriate anisotropy constants are not given by Eq. (7) but may be shown to be $a_{12}=-\omega_a$, $a_{21}=+\omega_a$.

IV. DETAILS OF EXPERIMENTS

Samples of single-crystal $RbMnF_3$[10] were cut in the form of 4-mm cubes, x-ray oriented and mounted to rotate about a [110] crystal axis. The sample shape is considered to be unimportant here. The convenient working temperature of 4.2°K, obtained by immersing the sample in liquid helium, brought both low- and high-field resonances into X band.

The sample was mounted at the movable end wall of a rectangular TE_{102} transmission cavity, tunable over X band. The applied dc field and the cavity rf field were in orthogonal directions in the corresponding (110) plane. The tuning adjustment was made at an applied field of 10 kOe, far from any observed resonances. Cavity output power was monitored on an XY recorder for increasing and decreasing field sweeps over a 0 to 10 kOe range. No difference was seen in the results. Precise determination of the location of the crystal axes to better than 0.5 deg with respect to the applied field was possible by observing the symmetry of the resonance spectrum as a function of orientation of $\mathbf{H}_0$ near to the [001] direction.

The observed resonances for the Sperry sample with $\mathbf{H}_0$ applied along the three principal axes are shown in Fig. 6. When $\mathbf{H}_0$ is parallel to the [001] axis, there are three modes clearly visible [Fig. 6(a)]. The low field branches converge to 9.23 GHz at $H_0=0$. The upper mode branch has a maximum value in frequency at a field of about 1.65 kOe. At higher fields the resonant frequency decreases, the resonance simultaneously decreasing in strength until it finally disappears at about 2.25 kOe. The resonances could not be observed below 8 GHz because of the limitations of the experimental arrangement. The high field mode, which was observable at field strengths above 3 kOe, follows an almost straight line having a slope of about 3.0 MHz per Oe. A typical plot of the relative power transmitted by the cavity as a function of $\mathbf{H}_0$ is shown in Fig. 7, for the frequency of 11.0 GHz. The two resonances on the left correspond to the upper branch of the low-field mode, while the third resonance belongs to the high-field mode.

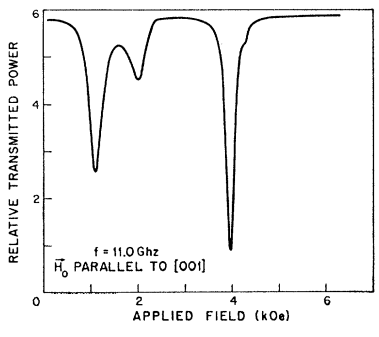

FIG. 7. An example of a resonance curve.

[10] The crystals used in the experiments were supplied by Dr. M. Kestigian of the Sperry Rand Research Center and by Dr. P. O. Henk of the Center for Materials Science and Engineering at MIT.

When the applied field is parallel to the [111] axis [Fig. 6(b)], only two mode branches are observed. The upper mode branch no longer exhibits a maximum value but with increasing field approaches asymptotically a straight line of positive slope. The slope of the lower branch appears to decrease in magnitude and approaches a constant frequency at high fields.

When $\mathbf{H}_0$ is parallel to the [110] axis, the mode spectrum, Fig. 6(c), is very different. A pair of modes is observable, but their intensities rapidly decrease when the field is raised above a few hundred oersteds. These resonances were very weak and were somewhat masked by a third very strong resonance which is also plotted in Fig. 6(c). The third resonance tends to a straight line of positive slope at high fields but with decreasing field approaches a constant frequency. All modes coalesce at the zero-field frequency of 9.23 GHz. For fields in excess of 3 kOe a resonant mode occurs almost identical to the one observed in Fig. 6(a) for the [001] case, but the resonance is very weak. We have been able to explain this resonance only by assuming a small portion of the crystal to have a different but related orientation to the major portion.

V. DISCUSSION OF RESULTS

For each of the crystals tested a good fit of the resonance theory to the experimental results could be obtained by adjusting the values of H_a and H_{ex}. The values obtained were $H_a=3.85\pm0.03$ Oe for the Sperry sample and $H_a=4.56\pm0.03$ Oe for the locally grown sample. Both crystals gave $H_{ex}=(8.9\pm0.05)\times10^5$ Oe, in agreement with published data.[5] The determination of these results requires the assumption of $H_n=2.24$ Oe from NMR measurements quoted by Teaney *et al.*,[1] which are presumed to be accurate.

The analysis of the equilibrium orientation has neglected energy terms resulting from shape-dependent demagnetizing effects. Such terms lead to a small correction in the fields corresponding to a given orientation and in particular to the field required for spin flopping, if any. For example, when $\mathbf{M}$ is along a [111] direction the field, H_0, for flopping is changed by the amount $H_0M/3H_{ex}$ for a spherical sample (a reasonable approximation for the actual sample shape used). Assuming the values $H_{ex}=8.9\times10^5$ Oe and $M=3.04\times10^5$ A/m the correction is equal to 300 A/m (3.75 Oe), and does not lead to any important changes in the expected behavior in the motion of the magnetization with applied field. Keffer and Kittel[9] have considered the effect of the demagnetizing fields upon the resonance spectrum of a uniaxial antiferromagnet and find that the corrections are correspondingly small.

It is interesting to note that the weak resonances corresponding to portions of the magnetization lying in equilibrium directions which are not the lowest energy could only be observed at low fields and for $\mathbf{H}_0$ lying along a [110] axis. This comes about because for $\mathbf{H}_0$ along the other axes, the stronger resonances caused by $\mathbf{M}$ in the lowest energy direction obscure the weaker ones. When $\mathbf{H}_0$ is along [110], the different tuning rates for the modes corresponding to $\mathbf{M}$ in different directions render them easier to distinguish. The low field modes die out above 450 Oe although the equilibrium analysis predicts that they should persist up to a field of 2.01 kOe.

Of particular interest is the prediction in the equilibrium analysis of two stable equilibrium directions for low fields applied in the [111] direction, and the associated resonance spectra. Efforts have been made to observe both these branches. First, to ensure that $\mathbf{M}$ lies along a [111] axis, a field of 10 kOe was applied along the direction orthogonal to [111], ($\theta=-35.3°$), and carefully reduced to zero magnitude. With the cavity tuned to a frequency of 8.4 GHz the sample was rotated to bring $\mathbf{H}_0$ along [111] and a field sweep from 0 to 10 kOe was taken. Only one resonance was observed; this corresponded to $\mathbf{M}$ close to those [111] directions not along $\mathbf{H}_0$. The simple model for the equilibrium orientation predicts that, with the appropriate prepositioning of $\mathbf{M}$ along the same [111] direction as $\mathbf{H}_0$, the field required for resonance with H_0 increasing from zero should be different from the value required when the resonance is approached from a high field. The failure of this type of behavior to emerge suggests that the magnetization can move from one energy minimum to a lower energy minimum by incoherent rotation at only moderate applied fields. The concept of spin flopping, valid for uniaxial and orthorhombic antiferromagnets[11] does not appear to apply in the case of $RbMnF_3$. If spin flopping in cubic antiferromagnets were to occur, it would be of an irreversible nature. In practical samples of $RbMnF_3$ it appears to be precluded by premature rotation of the magnetization by the above means.

ACKNOWLEDGMENT

We are pleased to acknowledge the continued interest of Professor D. J. Epstein and Professor F. R. Morgenthaler in this project. We are also indebted to Dr. P. O. Henk and Dr. M. Kestigian who grew the single crystals used. We wish to thank Dr. S. Foner for helpful criticism of the manuscript.

[11] T. Nagamiya *et al.*, Advan. Phys. 4, 1 (1955).